Dynamic Centrifuge Model Tests on Failure Behavior of Grid-Form DMWs Supporting a Tall Building

高層建物を支持する格子状地盤改良体の破壊挙動に関する動的な遠心実験

Junji Hamada 濱田 純次*1 Tsuyoshi Honda 本多 剛*1 Noriyuki Nakatsu 中津 紀幸*2

Summary

Two series of dynamic centrifuge model tests were conducted to investigate a failure behavior of grid-form DMWs (Deep cement Mixing Walls) in liquefiable sand during large earthquakes. In the first series, two types of DMWs models, which are acryl model and soil cement model with the rigid weight of 206 kPa, were set in a laminar shear box and tested in order to investigate influence of soil-cement's local yielding and failure on seismic performance by comparing to seismic responses of the both models. In second series, one soil-cement model with a natural period of 0.6 sec to 0.41 sec was also tested to reproduce a tall building. At the maximum input acceleration of 4.5 m/s^2, liquefaction was induced even in the area enclosed by DMWs and several cracks were locally induced in the soil-cement model. However, no significant settlement of the structure was observed even if the normal and shear stresses in the DMWs were assumed to have locally reached the tensile or shear criteria of soil-cement.

Keywords: grid-form deep mixing wall, centrifuge model test, failure of soil-cement, seismic behavior

梗　概

格子状地盤改良体の大地震時の破壊挙動を調べるために，2シリーズの遠心振動実験を行った。最初の実験は，改良体を模擬したアクリル模型とソイルセメントで作製した模型を同時に振動させて応答を比較することで，ソイルセメントの局所的な破壊が地震時性能に及ぼす影響を調べた。次に建物周期が約0.6秒と約0.41秒の建物（接地圧206kPa）を支持する格子状地盤改良体の挙動を調べた。入力加速度4.5m/s^{2}では，格子状地盤改良体で囲まれた地盤でも液状化が生じ，いくつかのクラックが見られ，部分的にソイルセメントの引張またはせん断強度に達していると考えられるが，顕著な沈下は生じなかった。

キーワード：格子状地盤改良，遠心実験，ソイルセメントの破壊，地震時挙動

1 INTRODUCTION

Grid-form DMWs (Deep cement Mixing Walls) were recently employed as a new method to increase bearing capacity of foundations in soft grounds as well as a countermeasure against seismic liquefaction. In the method, the high-modulus soil-cement walls confine the loose sand enclosed by the DMWs so as not to cause excessive shear deformation during an earthquake. Figure 1 shows schematic view of the DMWs and their construction procedure (Yamashita et al., 2011). The method was developed in the late 1980s, and has demonstrated that the grid-form DMWs effectively prevented liquefaction and liquefaction-induced damage in the 1995 Hyogoken-Nambu earthquake. Namely, during the earthquake, quay walls were heavily damaged due to liquefaction-induced lateral flow, however, a 14-story building with a foundation of cast-in-place concrete piles and the DMWs that was surrounded by the quay walls survived and no damage was observed in the pile foundation (Tokimatsu et al., 1996). In Japan, the grid-form DMWs have been widely used in a lot of buildings since 1995. The DMWs have been also applied to support buildings directly, and are capable of restricting the settlement of buildings during or after earthquakes to an

*1 Chief Researcher, Research & Development Institute, Dr. Eng. 技術研究所　主任研究員　博士（工学）
*2 Tokyo Main Office　東京本店　作業所

acceptable level. Recently piled raft foundations combined with the grid-form DMWs have been applied to the real buildings. The field measurements on long-term and seismic behaviors of the buildings supported by piled rafts with the DMWs were also performed to confirm the validity of their foundation designs (Yamashita et al., 2011, 2012, 2016). Furthermore, Tanikawa et al. (2015) proposed a mechanical joint adding dents and bumps at a top surface of the DMWs in order to ensure a transmitting large lateral forces such as unsymmetrical earth pressure or seismic inertia force of superstructure into the DMWs as shown in Fig. 2. The authors also proposed a calculation formula of prediction an ultimate lateral resistance of the joint and examined a cyclic loading tests to confirm shear failure of the joint and the validity of the proposed calculation formula.

Some researchers conducted numerical analyses using elasto-plastic models to investigate seismic behaviors of grid-form DMWs (Namikawa et al., 2007; Shigeno et al., 2017), and concluded that the local failures of the DMWs were not the causes of the reduction in the potential for liquefaction mitigation. However, the local failures of the DMWs are not acceptable in the existing method of allowable stress design. If a local failure can be appropriately taken into account, the DMWs can be designed more rationally, using a performance-based seismic design method. So far, a lot of shaking table tests on cement mixing walls have been carried out by using centrifuges (e.g., Babasaki et al., 1992). Most of them have been used acrylic resin models, the shear modulus of which is equivalent to that of real soil-cement in order to investigate an effect of preventing liquefaction during earthquakes. Several researchers recently conducted centrifuge model tests on grid-form DMWs using real soil-cement models (Tamura et al., 2015; Khosravi et al., 2016; Honda et al., 2015). Khosravi et al. (2016) used the soil-cement with an unconfined compressive strength of 450 to 770 kPa and investigated the effect of the area replacement ratio and improved depth on the global responses of the soft clay ground. Unfortunately, the above tests were conducted without setting superstructure models on the DMWs. Accordingly, they were not able to reach a conclusion about how the inertial force from superstructure affected the performance of the DMWs.

This paper describes two series of centrifuge model tests in 50 g field in order to investigate failure behavior of DMWs subjected to dynamic loading from superstructure and ground oscillation during large earthquake. In this study, the miniature model of DMWs was made of soil-cement in order to investigate the behavior/ toughness of the DMWs after yield and failure during large earthquakes. The relationship between shear stress and shear strain of the DMWs, namely the nonlinearity of the DMWs by gradually increasing the input motion step by step, was also investigated.

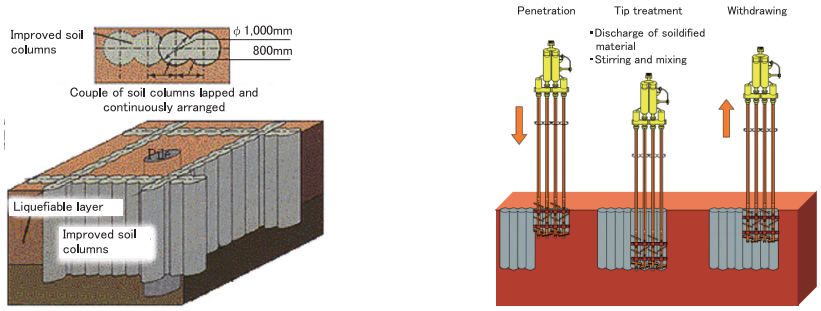

(a) Schematic view of DMWs (b) Construction procedure of DMWs

Fig. 1 Grid-form deep cement mixing walls (Yamashita et al., 2011)

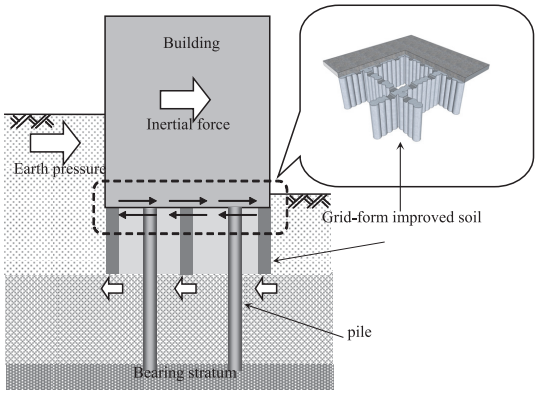

Fig. 2 Mechanical joints transmitting lateral to DMWs (Tanikawa et al., 2015)

2 CENTRIFUGE MODEL TESTS

Two series of centrifuge model tests were performed shown in Table 1. The tests were carried out at a centrifugal acceleration of 50 g using the 7 m radius centrifuge at Takenaka R & D Institute. The scaling ratio is 1/50. First series, shaking table tests using the acryl model and soil-cement model were simultaneously carried out to check the shear stiffness of the soil-cement model and to investigate a degree of yielding of it. The superstructure was modeled to be low rise building in this series. Next series, superstructure was modeled to be natural period of 0.6 sec to 0.41 sec in prototype scale. Both series of shaking table tests were conducted with liquefiable sand deposit. As the results, liquefactions weren't observed in series I, so water table level in series II was set higher than that in series I.

Table 1 Test Series and groud conditions

Test Case		DMws Model	Super structure	Maximum Input motion (cm/s^2)	Ground conditions	
					Water Level (in Proto.)	Relative density, Dr
Series I	Case 1	Acryl, Soil-cement	Low (rigid)	832	GL- 2.5 m	63%
Series II	Case 2	Soil-cement	Low (almost rigid)	482	GL- 1.0 m	72%
	Case 3		Natual period of 0.41 sec.	507		78%
	Case 4		Natual period of 0.60 sec.	477		76%

2.1 Series I tests at low-rise structure

2.1.1 Setting up model ground, dmws and structures

Figure 3 shows schematic view of the series I (Hamada and Honda, 2017). The DMWs models made of soil-cement and acryl resin were set in a laminar shear box, and a lot of accelerometers, piezometers and displacement transducers were set on the models, grounds and structures. The inner dimensions of the laminar shear box are 1000 mm long, 300 mm width, 350 mm height. A 2 mm-thick membrane was attached inside the box to make it watertight. Size of the both DMWs models are 20 mm thick of soil-cement wall (1.0 m thick in prototype scale) and spaced 240 mm center-to-center apart (12 m in prototype). Sand papers were attached on a top of the acryl model and beneath the steel structure models to increase a friction between the structure models and the DMWs.

Silica sand No.6 produced in Iide, Yamagata Prefecture, Japan was used as the soil for all test cases. The physical properties of the Iide sand are following; 50 percent diameter, D_{50} of 0.28 mm, uniformity coefficient, Uc of 1.9, specific gravity of soil particles of 2.657, minimum density of 1.452 g/cm^3, maximum density of 1.744 g/cm^3. Relative density of the saturated model ground is 63%. Model improved soil-cement walls were also made from Iide sand, kaolin clay and blast-furnace slag cement type B, W/C=60%. Unconfined compressive strength of the soil cement is from 1500 to 2000 kPa in curing time of 7 days and about 4000 kPa in curing time of 28 days.

Water table appears 2.5 m below the ground surface in prototype. Each structure model was made of two steel plates whose weight is 11.54 kg plus 16.89 kg, that correspond to a building average contact pressure of 206 kPa. Ground enclosed by DMWs was made by digging the ground about 5 mm so as not to contact the raft. So, whole inertial force of the structure can act directly to the DMWs.

Table 2 shows the test step numbers and the corresponding peak accelerations at the base (input), ground and structures at each step. Hereafter, test results are converted into the prototype scale. The TAFT wave was used as an input shaking motion throughout the tests (Series I and II). The wave's peak acceleration level was tuned from a small level to a large level, gradually increased step by step. Twenty test steps were conducted in order from above the table. Basically the input (base) accelerations were increased step by step, but several small input waves were provided at the steps 8 and 14 as intermediate steps in order to check the softening degree of the DMWs. If the DMWs were damaged, such damage should have appeared as a change of natural period of the structure.

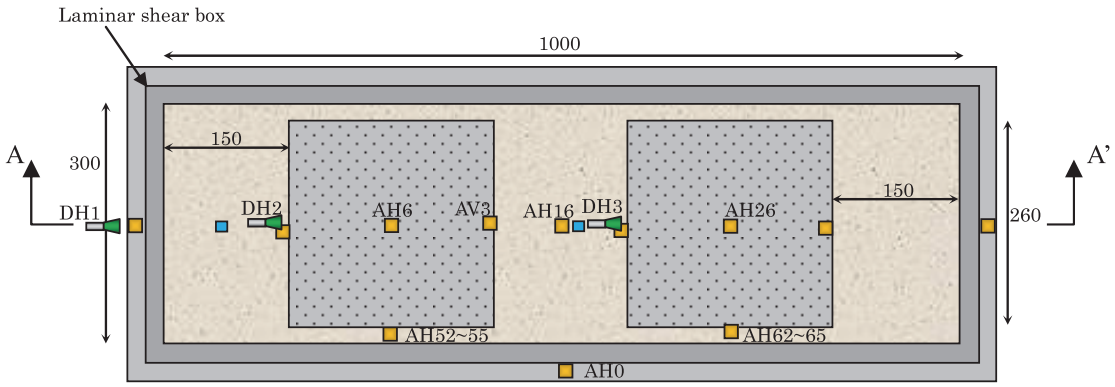

(a) Top view

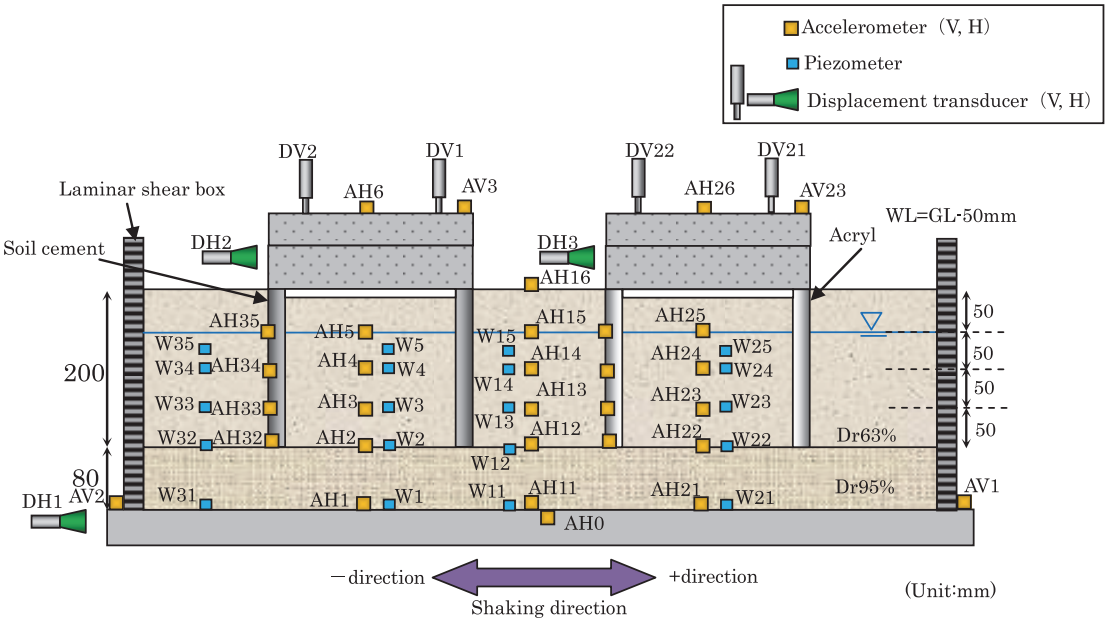

(b) Side view (A-A' cross section)

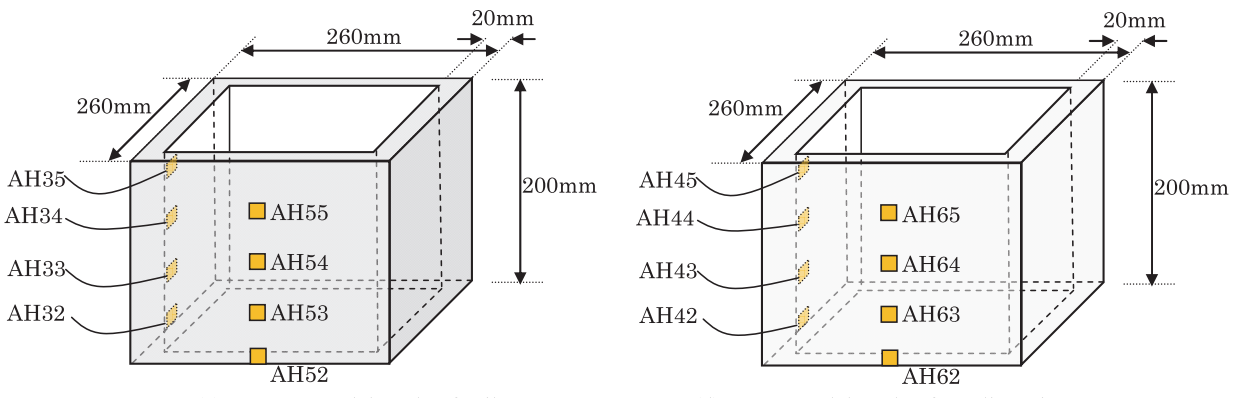

(c) DMW model made of soil-cement (d) DMW model made of acrylic resin

Fig. 3 Schematic views of series I models with rigid mass

2.1.2 Test results

Both peak ground accelerations (AH5, AH25) inside the DMWs made of soil-cement and acrylic resin remained almost the same until the step 14 as shown in Table 2. However, those inside the soil-cement DMWs were increased especially at and after the step 15. Table 2 also shows the residual settlements of the models. The parenthesized values are the integrated values from the beginning of the step 1. The settlements exceeded 100 mm in both the models.

Figures 4 and 5 show the time histories of the measured accelerations and excess pore water pressures respectively, at the step 5.

Table 2 Maximum accelerations and residual settlements (Case1, Series I)

Step number	Peak Acceleration (cm/s^2)										Residual settlement (mm)			
	Base	Ground			DMWs (Soil-cement)			DMWs (Acryl)			Soil-cement		Acryl	
		inner DMWs (Soil-cement)	inner DMWs (Acryl)	Free field	Transverse	Longitudinal	Structure	Transverse	Longitudinal	Structure				
	AH11	AH5	AH25	AH15	AH35	AH55	AH6	AH45	AH65	AH26	DV2	DV1	DV22	DV21
1	53	53	56	56	57	49	100	50	52	88	2.3	3.7	1.4	1.5
2	100	78	78	88	86	78	142	87	76	141	7.3 (9.6)	5.1 (8.8)	4.8 (6.2)	3.5 (4.9)
3	113	94	92	141	95	92	165	104	88	174	3.6 (13.2)	4.7 (13.5)	2.1 (8.3)	3.7 (8.6)
4	140	97	102	128	111	109	185	113	103	200	4.2 (17.4)	3.8 (17.4)	3.4 (11.7)	3.1 (11.7)
5	174	115	120	137	127	121	211	131	122	221	7.6 (25.1)	4.4 (21.7)	4.5 (16.2)	6.3 (18.0)
6	202	136	137	147	151	134	235	143	135	242	5.2 (30.3)	6.8 (28.5)	4.9 (21.1)	6.3 (24.3)
7	245	157	144	165	166	153	248	159	153	269	7.5 (37.8)	6.4 (34.9)	4.6 (25.8)	5.6 (29.9)
8	75	83	122	109	85	77	136	91	72	113	0.3 (38.1)	0.5 (35.4)	0.7 (26.5)	0.2 (30.1)
9	256	178	160	197	198	167	274	188	158	289	6.7 (44.8)	6.7 (42.1)	5.9 (32.4)	5.8 (35.9)
10	333	211	185	219	232	206	300	197	192	311	9.3 (54.1)	7.6 (49.7)	6.7 (39.1)	6.5 (42.4)
11	368	244	226	256	242	211	323	264	217	340	14.0 (68.1)	9.7 (59.4)	5.8 (44.8)	9.3 (51.7)
12	426	292	286	300	274	222	352	307	234	371	11.5 (79.6)	10.7 (70.1)	7.0 (51.9)	5.4 (57.1)
13	407	396	306	323	305	255	379	369	273	396	12.3 (92.0)	9.1 (79.2)	6.6 (58.4)	8.5 (65.6)
14	85	99	84	121	89	82	134	87	76	108	-0.5 (91.4)	0.3 (79.5)	-0.8 (57.7)	-0.2 (65.4)
15	489	793	367	368	412	273	419	457	423	441	11.6 (103.0)	10.1 (89.7)	8.8 (66.5)	9.1 (74.5)
16	530	1288	424	420	534	320	451	536	450	473	11.9 (114.9)	9.0 (98.6)	7.0 (73.5)	7.7 (82.2)
17	635	1288	489	562	643	372	485	487	572	515	9.5 (124.4)	9.4 (108.0)	8.9 (82.3)	11.2 (93.4)
18	715	1176	631	773	820	431	524	607	552	580	13.8 (138.2)	11.6 (119.6)	11.8 (94.1)	12.0 (105.4)
19	832	1289	627	608	821	430	581	732	598	583	8.5 (146.8)	7.1 (126.7)	8.8 (102.9)	9.1 (114.5)
20	581	333	368	346	349	321	423	418	446	384	0.6 (147.4)	1.1 (127.8)	-0.4 (102.5)	1.0 (115.5)

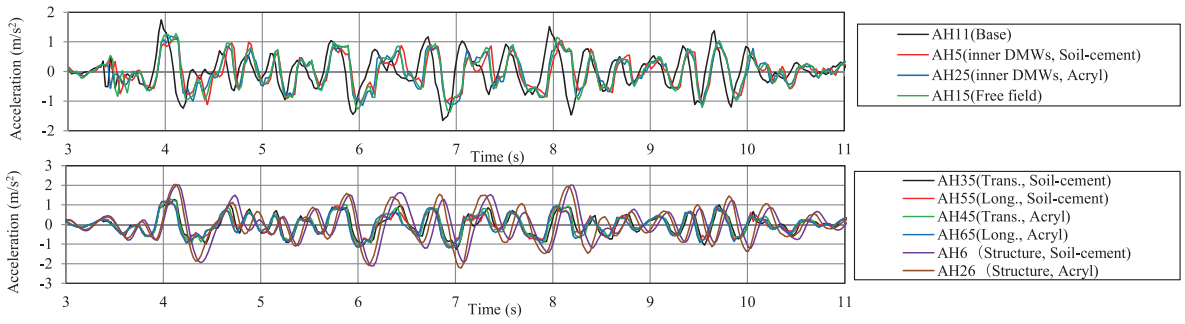

Fig. 4 Time histories of measured accelerations (step 5)

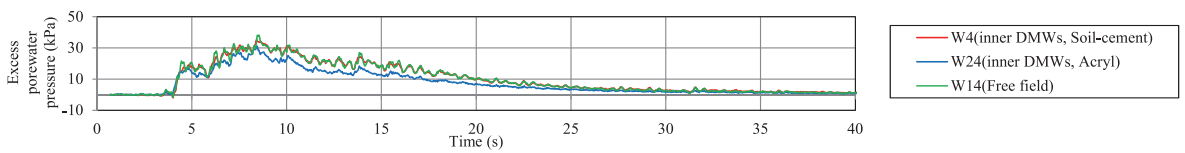

Fig. 5 Time histories of measured excess pore water pressures (step 5)

Figures 6 and 7 show those at the step 15. At the step 15, the acceleration inside soil-cement DMWs, AH5, had several sharp peaks after t=5.8 s, where the acceleration of the transverse wall, AH35, made of soil-cement became larger than the longitudinal wall, AH55. The excess pore water pressure inside soil-cement DMWs, W4, was larger than the one inside acrylic DMWs, which however, were not liquefied.

Both structure models (AH6, AH26) behaved similarly when an input acceleration was over 4.8 or 8 m/s^2. Other results of Series I are described in reference (Hamada and Honda, 2017).

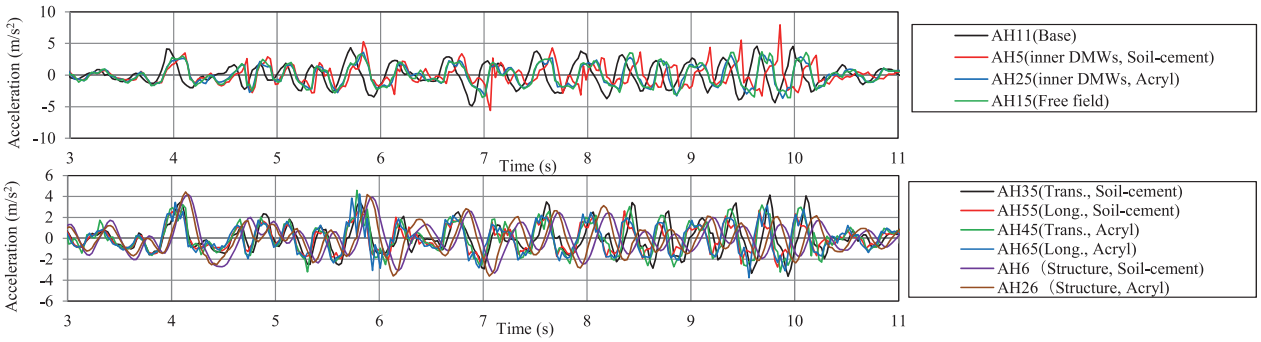

Fig. 6 Time histories of measured accelerations (step 15)

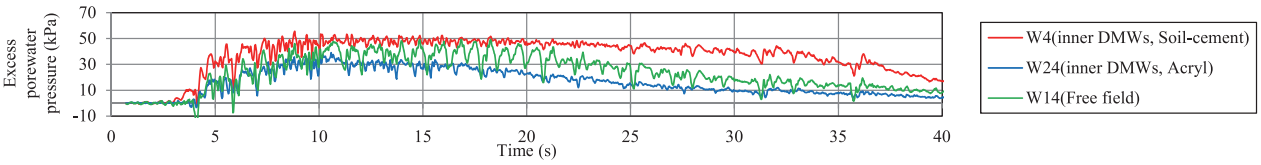

Fig. 7 Time histories of measured excess pore water pressures (step 15)

2.2 Series II tests at high-rise structure

2.2.1 Setting up model ground, DMWs and structures

Next series, shaking table tests with liquefiable sand deposit were conducted. Liquefactions weren't observed in series I, so water table level in series II was set higher than that in series I. Superstructure was modeled to be natural period of about 0.6 sec in prototype scale. Figure 8 shows schematic view of the series II. The DMWs models made of soil-cement with superstructure was set in a center of the laminar shear box, and a lot of accelerometers, piezometers and displacement transducers were set on the model, grounds and structure. Sizes of the DMWs model and how to make it are same as those in series I. Relative density of the model sand is 72% to 78%.

Sand papers were attached on a bottom of the steel structure model in the same way as series I. Water table appears 1.0 m below the ground surface in prototype. Superstructure model's weight and substructure's one are 11.54 kg and 16.89 kg, respectively. That corresponds to a building average contact pressure of 206 kPa. Ground enclosed by DMWs was made by digging the ground about 5 mm so as not to contact the raft. So, whole inertial force of the structure can act directly to the DMWs.

Table 3, 4 and 5 show test step numbers and corresponding maximum accelerations at base (input), grounds and structures on each steps at Cases 2, 3 and 4, respectively. Five test steps were conducted in order from above of each table. The acceleration at the superstructure did not amplified from basement at Case 2, so those of the basement occurred larger than those at Cases 3 and 4.

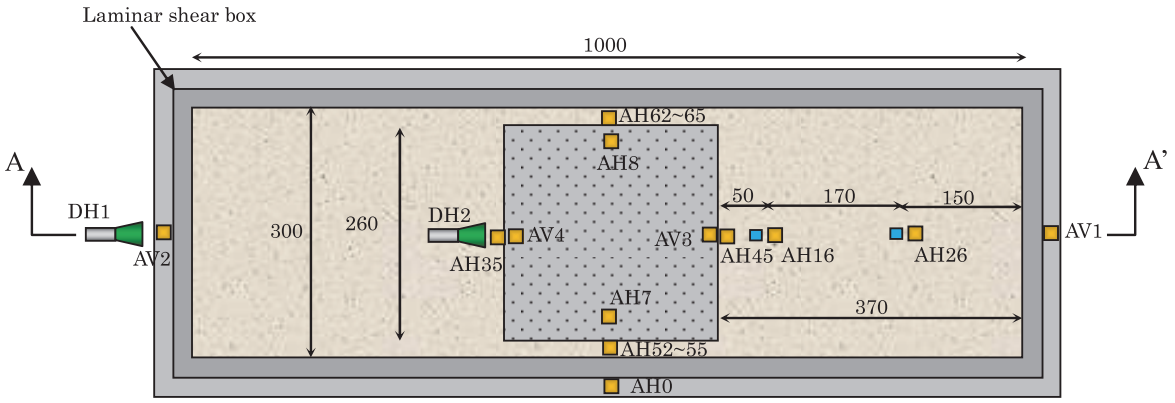

(a) Top view

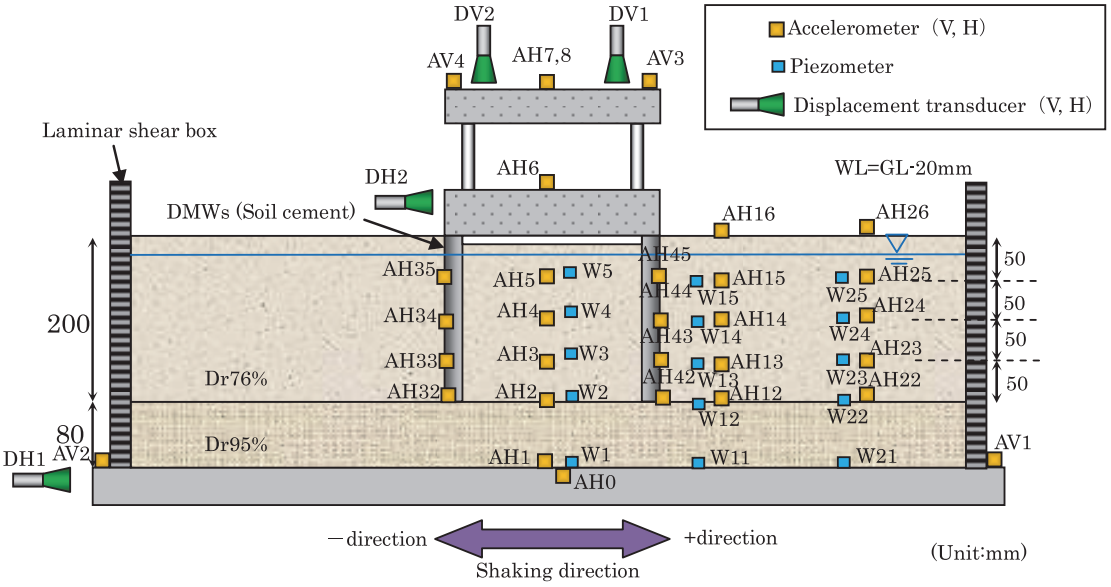

(b) Side view (A-A' cross section)

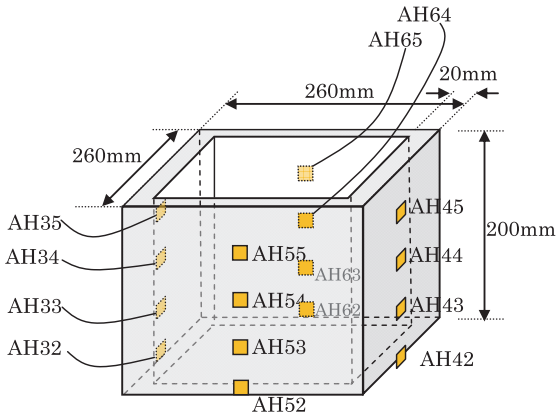

(a) DMWs model

Fig. 8 Schematic view of series II with high-rise building

Table 3 Maximum accelerations and residual settlements (Case 2, Series II)

Step number	Peak Acceleration (cm/s^2)							Residual settlement (mm)	
	Base	Ground		DMWs		Structure		Structure	
		inner DMWs	Free field	Transverse	Longitudinal	Basement	superstructure		
	AH1	AH5	AH25	AH35, AH45	AH55, AH65	AH6	ave. (AH7, AH8)	DV1	DV2
1	94	98	102	69, 62	61, 60	95	108	-0.1	-0.3
2	173	149	127	160, 147	129, 122	185	206	3.4 (3.3)	3.5 (3.2)
3	205	187	186	179, 165	146, 146	224	249	4.1 (7.5)	3.9 (7.1)
4	333	663	501	292, 295	204, 205	300	324	15.9 (23.4)	15.4 (22.5)
5	482	887	653	548, 456	218, 210	346	378	26.7 (50.1)	25.0 (47.5)

Table 4 Maximum accelerations and residual settlements (Case 3, Series II)

Step number	Peak Acceleration (cm/s^2)							Residual settlement (mm)	
	Base	Ground		DMWs		Structure		Structure	
		inner DMWs	Free field	Transverse	Longitudinal	Basement	superstructure		
	AH1	AH5	AH25	AH35	AH65	AH6	ave. (AH7, AH8)	DV1	DV2
1	72	68	68	67	56	75	166	1.8	2.4
2	255	236	123	195	148	155	296	13.2 (15.0)	13.5 (16.0)
3	217	421	288	240	182	196	334	8.8 (23.8)	8.3 (24.3)
4	365	857	767	454	286	251	448	26.3 (50.1)	24.4 (48.7)
5	507	906	781	745	343	255	528	28.7 (78.8)	26.6 (75.3)

Table 5 Maximum accelerations and residual settlements (Case 4, Series II)

Step number	Peak Acceleration (cm/s^2)							Residual settlement (mm)	
	Base	Ground		DMWs		Structure		Structure	
		inner DMWs	Free field	Transverse	Longitudinal	Basement	superstructure		
	AH1	AH5	AH25	AH35, AH45	AH55, AH65	AH6	ave. (AH7, AH8)	DV1	DV2
1	51	67	73	70, 67	63, 61	68	160	1.9	1.9
2	163	162	185	168, 162	137, 131	153	313	16.7 (18.6)	18.1 (20.0)
3	197	210	386	215, 212	165, 156	186	391	10.1 (28.7)	10.2 (30.3)
4	347	334	418	317, 322	195, 213	215	501	35.5 (64.2)	34.1 (64.4)
5	477	511	759	412, 448	239, 235	238	519	37.5 (101.7)	36.2 (100.6)

2.2.2 Test results

Table 3, 4 and 5 also show residual settlements of the models. The values in parentheses are integrated values from beginning of step 1. At Case 4, the settlements reached over 100 mm after the step 5 which correspond to the step 15 at series I. Figure 9 and 10 show time histories of measured accelerations and excess pore water pressures at Case 4, respectively at step 2 when liquefaction was observed outside the DMWs, W24 and W14. And Fig. 11 and 12 show those at step 5 when liquefaction was observed even in the area enclosed by DMWs, W4. It was observed phase difference between vibrations of the superstructure and the ground because natural period of the superstructure model, about 0.6 sec is larger than predominant period of the ground, about 0.45 sec.

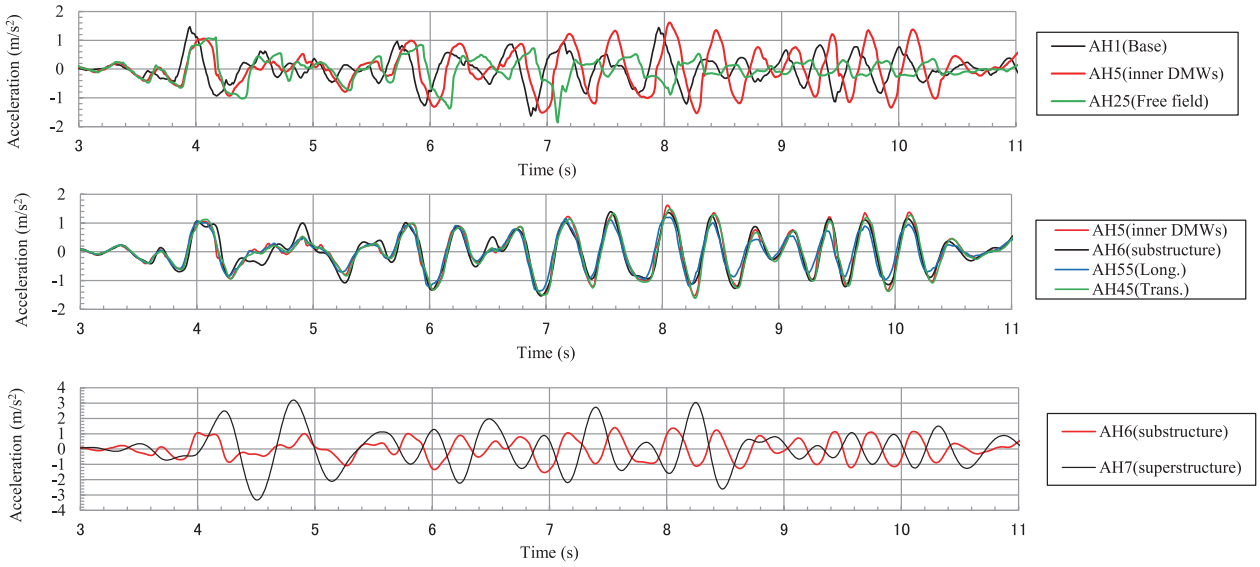

Fig. 9 Time histories of measured accelerations (step2) (Case 4, Series II)

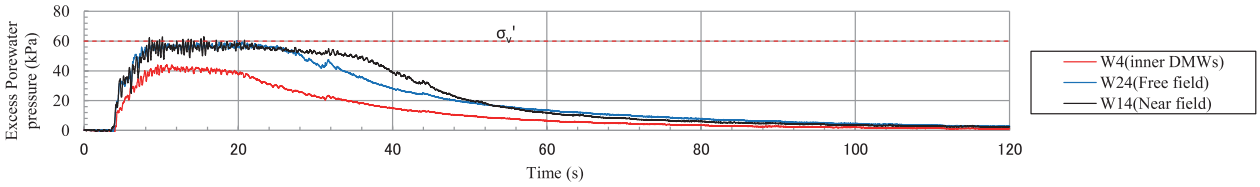

Fig. 10 Time histories of measured excess pore water pressures (step2) (Case 4, Series II)

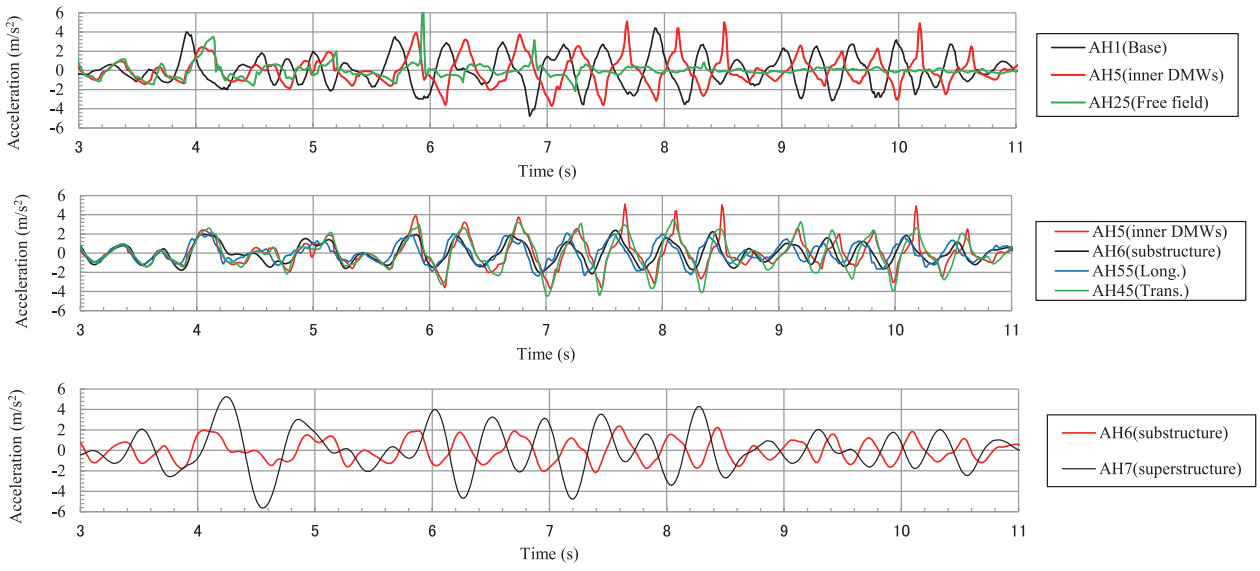

Fig. 11 Time histories of measured accelerations (step5) (Case 4, Series II)

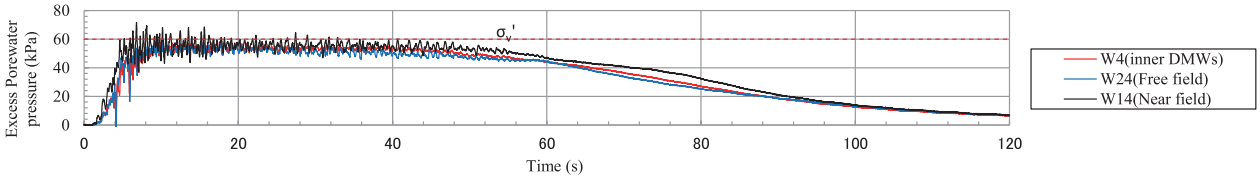

Fig. 12 Time histories of measured excess pore water pressures (step5) (Case 4, Series II)

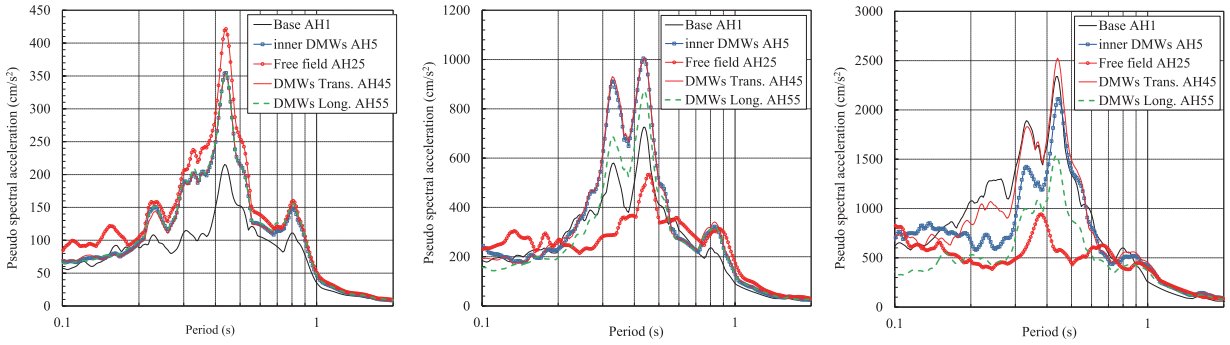

(a) Step 1 (b) Step 2 (c) Step 5

Fig. 13 Acceleration response spectra (5 % damping) (Case 4, Series II)

Acceleration response spectra (linear elastic, 5% damping) for measured motions in step 1, 2 and 5 are shown in Fig. 13. At step 1, the responses of DMWs, AH45, AH55 and ground enclosed by it, AH5 were almost the same, and the response at free field was slightly larger than that at ground enclosed by DMWs. In step 2, liquefaction occurred at free field, thereby the response at free field increased at long-period region. The responses of ground enclosed by DMWs, AH5 and transvers wall of DMWs, AH45 were similar, however the one of longitudinal wall, AH55 was slightly smaller than those. In step 5, liquefaction occurred even in the area enclosed by DMWs, the response of longitudinal wall, AH55 became smaller than one of the base, AH1 in the range under 0.9 sec.

Figure 14 (a) shows the relationship between the shear strain of the inner ground at the soil-cement model, γ_{eg_soil} and the shear stress of the whole improved ground at the soil-cement model, τ_{eg_soil}. The inertial forces of structure and soil enclosed by the DMWs were assumed to be the lateral load acting on the DMWs. These values are defined as follows:

$$\gamma_{eg\_soil} = (\delta_{AH5}\text{-}\delta_{AH2})/h \quad (1)$$

$$\tau_{eg\_soil} = ((a_{AH7} + a_{AH8})/2 \times m_{s1} + a_{AH6} \times m_{s2} + a_{AH5} \times m_{g5} + a_{AH4} \times m_{g4} + a_{AH3} \times m_{g3} + a_{AH2} \times m_{g2})/A_{Whole} \quad (2)$$

where δ_{AHi} is a displacement at the point of AHi calculated by double integrations from the measured acceleration of a_{AHi} using the frequency components from 20 Hz to 0.05 Hz; a_{AHi} is an acceleration at the point of AHi shown in Fig. 8; h is a distance between accelerometers; m_{s1} is a mass of superstructure; m_{s2} is a mass of substructure and $m_{g5\text{-}2}$ is a mass of ground separated to each layer of 5, 4, 3 and 2.

h = 7.5 m
m_{s1} = 1442 ton
m_{s2} = 2111 ton
m_{g5} = 4.25 m × A_{Whole} × ρ_s = 1458 ton
$m_{g4} = m_{g3}$ = 2.5 m × A_{Whole} × ρ_s = 857 ton
m_{g2} = 1.75 m × A_{Whole} × ρ_s = 600 ton
A_{Whole} = 13 m × 13 m = 169 m^2
ρ_s = 2.03 t/m^3

Figure 14 (b) shows the relationship between the shear strain of the longitudinal DMWs, γ_{DMW} and the assumed shear stress of the longitudinal DMWs, τ_{DMW}. It is assumed that lateral load was supported only by two sheets of longitudinal DMWs. These values are defined as follows:

$$\gamma_{DCM} = (\delta_{AH55}\text{-}\delta_{AH52})/h \quad (3)$$

$$\tau_{DCM} = ((a_{AH7} + a_{AH8})/2 \times m_{s1} + a_{AH6} \times m_{s2} + a_{AH5} \times m_{g5} + a_{AH4} \times m_{g4} + a_{AH3} \times m_{g3} + a_{AH2} \times m_{g2})/A_{DMW\_L} \quad (4)$$

where

A_{DMW_L} = 13 m × 1 m × 2 sheets = 26 m^2

Hyperbolic curves (HD model) estimated by the initial shear stiffness of 800 MPa, and the ultimate shear stress of 1200 kPa (0.3 *Fc*, where *Fc* = 4000 kPa) were also described in Fig. 14 (b).

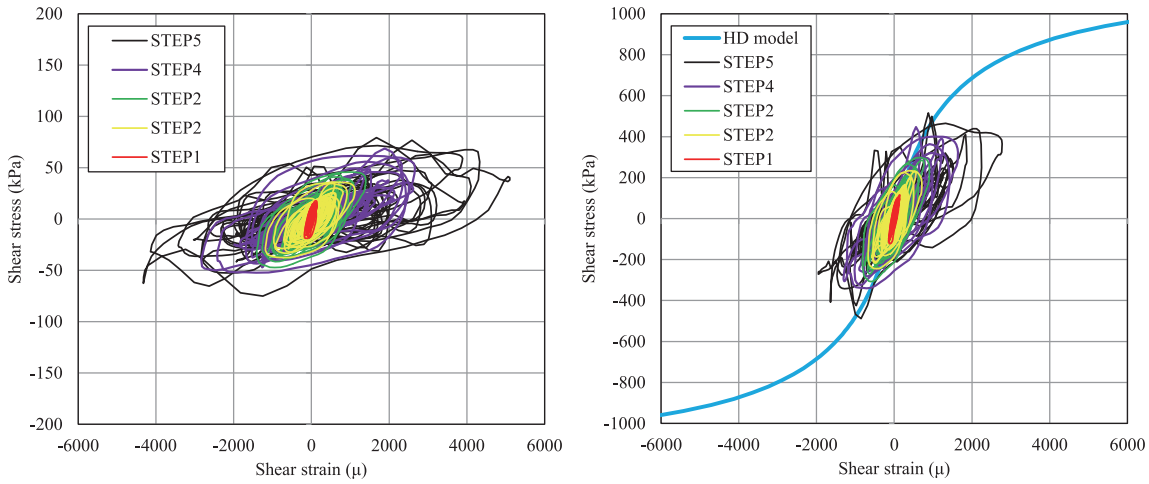

(a) Whole improved ground (b) Longitudinal DMWs

Fig. 14 Relationship between shear strain and shear stress (Case 4, Series II)

Figure 15 shows time histories of shear stress of the longitudinal DMWs, τ_{DMW} generated by inertial force of structure, $\tau_{DCM\_structure}$, (Equation (4')) and inertial force of enclosed soil, τ_{DCM_ground}, (Equation (4")) at step 2. The each components of the shear stress oscillate with phase difference.

$$\tau_{DCM\_structure} = ((a_{AH7} + a_{AH8})/2 \times m_{s1} + a_{AH6} \times m_{s2})/A_{DMW\_L} \quad (4')$$

$$\tau_{DCM\_ground} = (a_{AH5} \times m_{g5} + a_{AH4} \times m_{g4} + a_{AH3} \times m_{g3} + a_{AH2} \times m_{g2})/A_{DMW\_L} \quad (4'')$$

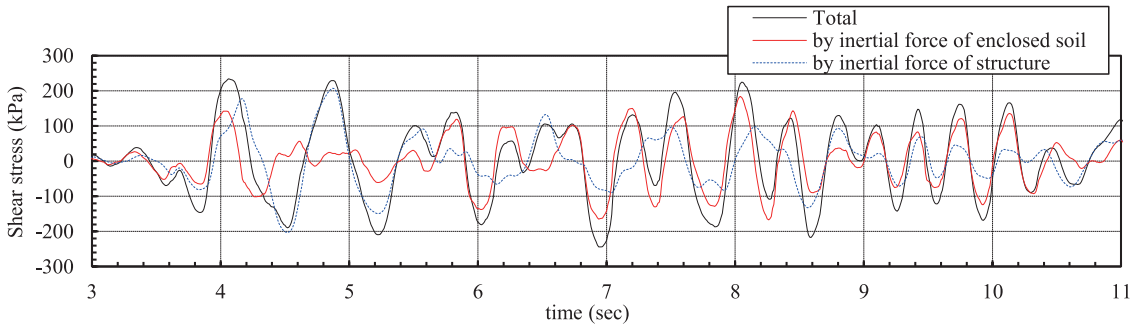

Fig. 15 Time history of components of shear stress of longitudinal DMWs (step 2, Case 4, Series II)

Photo 1 shows the DMW model made of soil-cement after shaking tests of Case 3. The photo (a) in Photo 1 shows the top view of the DMWs. The cracks on the longitudinal wall and transverse walls can be seen. The photos (b) and (c) in Photo 1 show the outside views of the transverse walls after removing model sand. Obvious cracks were observed at center part of the both transvers walls. The photo (d) in Photo 1 shows the inside views of the longitudinal wall after removing model sand and clear crack was observed. The crack width seems relatively large in photo (d), but the width was expanded when the model sand was removed after the tests. It is considered that the cracks of the longitudinal walls were caused by the inertial force of structure and it is presumed that the cracks in transverse walls were caused by either or both of the deformations of the inner ground enclosed by DMWs and the outside ground.

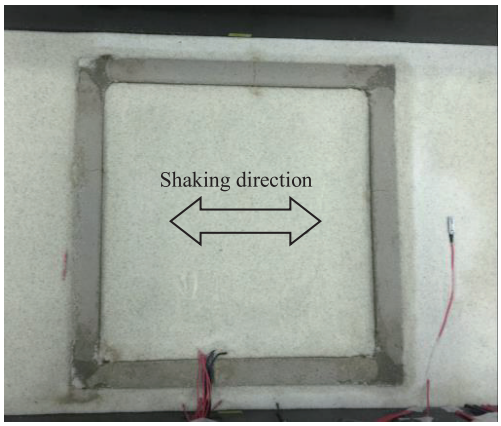

(a) Top view of the DMWs

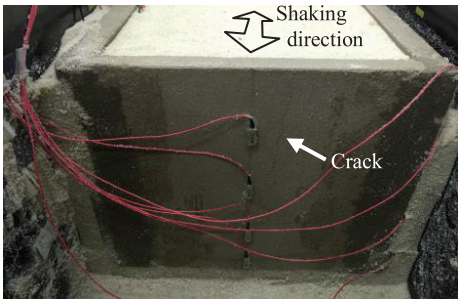

(b) Transvers wall of the DMWs

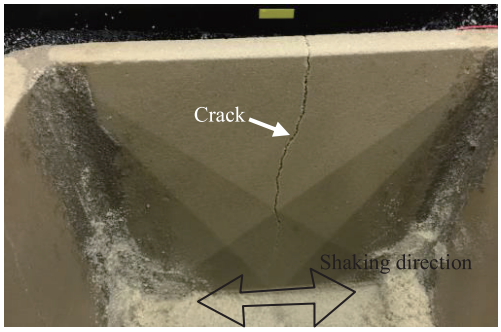

(d) Longitudinal wall of the DMWs

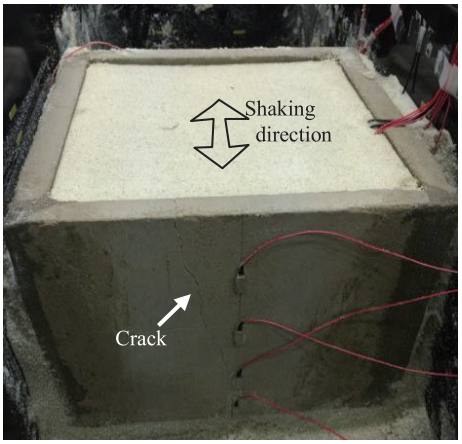

(c) Transvers wall of the DMWs

Photo 1 Observed cracks in DMWs model after shaking tests (Case3, Series II)

3 CONCLUSUIONS

Two series of centrifuge model tests in 50 g using saturated liquefiable model sand with grid-form DMWs have been carried out in order to investigate a failure behavior of DMWs subjected to dynamic loading during large earthquake.

In series I, DMW models made of acrylic resin and real soil-cement were simultaneously vibrated to check the shear stiffness of the soil-cement model and degree of yielding of the soil-cement model. Both models behaved similarly when an input acceleration was over 4.8 or 8 m/s^2.

In series II at case 4, liquefaction wasn't observed in enclosed sand deposit by DMWs when the maximum acceleration of the input motion was 1.5 m/s^2, however it was observed outside the DMWs. When the maximum input acceleration was 4.5 m/s^2, it was observed even inner enclosed sand deposit by DMWs and the cracks of the DMWs would occur. It was not observed significant settlement of the structure even if the stress reached to tensile or shear criteria at a part of the grid-form DMWs.

Several cracks of the soil-cement model were observed after repetitive shaking tests including input motion over 4.5 m/s^2. Those cracks were visually observed. A relatively large crack occurred at longitudinal walls, and relatively small cracks were observed at transvers wall. It is considered that the cracks of the longitudinal walls were caused by the inertial force of structure, and the cracks of transverse walls were caused by either or both of the deformations of the inner ground enclosed by DMWs and the outside ground. No significant settlement was observed in the tested structure though the stress reached tensile or shear criteria at a part of the grid-form DMWs.

ACKNOWLEGEMENTS

The authors are grateful to Dr. K. Yamashita of Takenaka R & D Institute for his constructive comments on the experimental results.

REFERENCES

Babasaki, R., Suzuki, K. and Suzuki, Y., 1992. Centrifuge tests on improved ground for liquefaction, *Proc. 10th WCEE, Balkema, Rotterdam, Netherlands*, 1461-1464.

Hamada, J. and Honda, T., 2017. Centrifuge model tests on failure behavior of grid-form deep mixing walls during large earthquake, *16WCEE* (contributing).

Honda, T., Hamada, J. and Nakatsu, N., 2015. Centrifuge model tests on dynamic performance of grid-form soil improvement walls, *50th Annual Convention of Japanese Society of Soil Mechanics and Foundation Engineering*, 1259-1260 (in Japanese).

Khosravi, M., Boulanger, R. W., Tamura, S., Wilson, D. W., Olgun, C. O. and Wang, Y., 2016. Dynamic centrifuge tests of soft clay reinforced by soil-cement grids, *J. Geotech. Geoenviron. Eng*.

Namikawa, Y., Koseki, J. and Suzuki, Y., 2007. Finite element analysis of lattice-shaped ground improvement by cement-mixing for liquefaction mitigation, *Soils & Foundations*, Vol.47, No.3, 559-576.

Shigeno, Y., Hamada, J., Yamashita, K. and Nakamura, N., 2017. Numerical analyses of a piled raft foundation with grid-form DMWs under large earthquake load, *16WCEE* (contributing).

Tamura, S., Khosravi, M., Boulanger, R. W., Wilson, D. W., Olgun, C. G., Rayamajhi, D. and Wang, Y., 2015. Site response of soft clay reinforced by soil-cement grid based on dynamic centrifuge tests, *6th International Conference on Earthquake Geotechnical Engineering*.

Tanikawa, T., Hamada, J. and Honda, T., 2015. Mechanical joint transmitting lateral force to grid-form soil improvement, *the 15th Asian Regional Conference on Soil Mechanics and Geotechnical Engineering*.

Tokimatsu, K., Mizuno, H. and Kakurai, M., 1996. Building damage associated with geotechnical problems. *Special Issue of Soils & Foundations*, 219-234.

Yamashita, K., Hamada, J. and Yamada, T., 2011. Field measurements on piled rafts with grid-form deep mixing walls on soft ground, *Geotechnical Engineering Journal of the SEAGS & AGSSEA*, Vol.42, No.2, 1-10.

Yamashita, K., Hamada, J., Onimaru, S. and Higashino, M., 2012. Seismic behavior of piled raft with ground improvement supporting a base-isolated building on soft ground in Tokyo, *Soils & Foundations*, Vol.52, No.5, 1000-1015 Special issue on Geotechnical Aspects of the 2011 off the Pacific coast of Tohoku Earthquake.

Yamashita, K., Hamada, J. and Tanikawa, T., 2016. Static and seismic performance of a friction piled raft with deep mixing walls in soft ground in Tokyo, *Soil & Foundations*, Vol.56, No.3, 559-573.